International Journal of Environmental Science and Technology
https://doi.org/10.1007/s13762-024-05905-0

ORIGINAL PAPER

Rotor–stator hydrodynamic cavitation reactor for intensification of castor oil biodiesel production

M. Khater[1] · O. Aboelazayem[2] · A. R. Ismail[3] · A. Soliman[1] · S. A. Abu Amr[4] · N. Sh. El-Gendy[3,5] · A. A. Ezzat[1]

Received: 25 January 2024 / Revised: 22 June 2024 / Accepted: 11 July 2024

Abstract

Nowadays, the intensification of the production of biodiesel from non-edible oil crops is mandatory to overcome petrol-fuel depletion and environmental pollution. For the first time, enhanced biodiesel production from castor oil via rotor–stator hydrodynamic cavitation has been studied in this work. Response surface methodology based on one-factor-at-a-time design of experiments was employed for modelling and optimizing the biodiesel yield and the decrease in feedstock viscosity, density, and total acid number (TAN). The predicted optimum parameters of 8.15:1 methanol:oil (M:O), 1499 rpm, 29.38 min, 48.43 °C, and a KOH catalyst concentration of 0.74 wt.% resulted in a 96% biodiesel yield with a concomitant decrease in viscosity, density, and TAN of approximately 95%, 5.12%, and 90.02%, respectively. According to the results of the breakthrough kinetic calculations, the reaction is pseudo-second order, with the activation energy, frequency factor, and reaction rate constant being 0.23 M^{-1} min^{-1}, 18.77 kJ/mol, and 6.32 M^{-1} min^{-1}, respectively. The fuel properties of the produced biodiesel and bio-petro-diesel blends were good, comparable to international standards and the marketed Egyptian petro-diesel.

Keywords Rotor–stator hydrodynamic cavitation reactor · Castor oil transesterification · Process optimization · Process kinetics and thermodynamics · Biodiesel intensification

Introduction

Diesel fuel is essential to the economy, industrial activities, transportation, the agricultural sector, and the fulfilment of many other fundamental human requirements in contemporary society. Experts estimate that the petition for liquid fuels worldwide will rise by 32% between 2020 and 2050 (Xu et al. 2022). Diesel fuel combustion contributes to the problem of climate change via enhanced greenhouse gas (GHG) emissions, in addition to SOx, NOx, and particulate matter, which leads to severe health and environmental issues (Reşitoğlu et al. 2015). For many years, biodiesel has emerged as a compelling complementary and/or substitute for traditional diesel fuel (Gholami et al. 2021). Biodiesel's power and torque characteristics, similar to those of conventional diesel, allow for its utilization in diesel engines with little to no engine modification needed (Aboelazayem et al. 2018; Tamilvanan et al. 2022). Furthermore, because of its molecular oxygen content, it offers superior combustion characteristics to ordinary petro-diesel (Tamilvanan et al. 2022). Additionally, biodiesel is biodegradable, meaning that if it is accidentally released into the environment, it will have a low negative impact on the ecosystem (Khater et al. 2023). The technical benefits of biodiesel over conventional diesel are numerous and include reduced exhaust emissions, low toxicity and carbon footprint, superior flash point and lubricity, low sulfur content, and the fact that it is derived

Editorial responsibility: Maryam Shabani.

✉ N. Sh. El-Gendy
nourepri@yahoo.com

1 Faculty of Engineering, Pharos University in Alexandria, PO Box 37, Sidi Gaber, Alexandria, Egypt

2 School of Computing, Engineering and Digital Technologies, Teesside University, Middlesbrough TS13BX, UK

3 Egyptian Petroleum Research Institute (EPRI), Nasr City, Cairo PO 11727, Egypt

4 Health Safety and Environmental Management, International College of Engineering and Management, 111 Seeb, PO 2511 Muscat, Oman

5 Center of Excellence, October University for Modern Sciences and Arts (MSA), 6th of October City, Giza PO 12566, Egypt

Published online: 12 August 2024

from a domestic and renewable feedstock (Hanif et al. 2022). Oil crop-derived biodiesel is reported to emit 63% lower GHG than petro-diesel (Xu et al. 2022), with a net reduction in emitted CO_2 of 78.45% (Sheehan et al. 1998). However, the efficiency of the transesterification of oil feedstock into biodiesel is one of the major bottlenecks in the biodiesel industry. It should be efficient enough to reduce, as much as possible, the fatty acid content and viscosity to the international permissible standard specifications (EN14214 and ASTM-D6751). Otherwise, engines operating on low-qualified biodiesel that exceeds the permissible range of viscosity or total acid number may experience operational issues over time (Tamilvanan et al. 2022).

Diesel and biodiesel blends have been extensively utilized. Cleaner emissions with fewer soot particles and whiter smoke will result from the use of biodiesel/petro-diesel blends (Farvardin et al. 2022). Moreover, it reduces engine wear and emits fewer sulfur dioxide and greenhouse gas (GHG) emissions (Aboelazayem et al. 2018).

Since castor oil is inedible, it poses no threat to the food industry and has the potential to be a valuable feedstock for the manufacturing of biodiesel (Angassa et al. 2023). Not only that, but also the cost of producing castor seeds is lower than that of producing soybean, rapeseed, and jatropha (Carrino et al. 2020). Castor plants require little water, can grow on harsh lands, can withstand drought and salinity, and are resistant to pests. Moreover, castor plants grow naturally as an association species in various environments along Nile River and deserts in Egypt, with an annual seed production that would exceed 250,700 tonnes (Aboelazayem et al. 2018). When compared to other world-wide-grown oil crops like soybean (15–20%), sunflower (25–35%), rapeseed (38–46%), and palm (30–60%), castor seeds have a very high oil content of 40–60% (Khater et al. 2023). Its high concentration of ricinoleic acid makes it suitable for industrial uses rather than culinary ones (Mubofu 2016). It has been recently reported for the phytoremdiation of polluted soil (Bauddh and Singh 2012). Thus, castor is considered a win–win solution for soil reclamation as well as a sustainable feedstock for biodiesel production.

There are several methods for biodiesel production: the conventional mechanical stirring technique (El-Gendy et al., 2014), ultrasonic cavitation (Ortega-Alegria and Floréz-Marulanda 2019), microwave, supercritical methanol, and hydrodynamic cavitation (Ghayal et al. 2013). Researchers have reported that the intensification hydrodynamic cavitation process is energy-efficient, easy to use, rapid, economical, environmentally benign, and can be easily scaled up (Yusup et al. 2015). It has been reported to decrease energy consumption by 40% relative to conventional mechanical stirring technology (Innocenzi and Prisciandaro 2021). Cavitation is a technique for transforming mechanical energy into high-kinetic energy. This energy is then released in brief bursts and can be used to boost green processes (Samani et al. 2021). As a result, it is based on a chain of the formation and collapse of millions of cavitation bubbles between alcohol and oil, resulting in massive localised turbulence, the removal of mass transfer limitations, an increase in reactant contact surface area, and subsequent improvements in the transesterification reaction (Wu et al. 2019). There are many publications concerning the applications of orifice- or venture-hydrodynamic cavitation reactors in the intensification of biodiesel production (Pal et al. 2010; Ghayal et al. 2013; Chuah et al. 2015; Kolhe et al. 2017; Chitsaz et al. 2018; Mistry et al. 2019; Khan et al. 2020; Asif et al. 2021a,b; Vera-Rozo et al. 2022; Hamidi et al. 2023). However, there is limited publication on the application of stator-rotor type hydrodynamic cavitation reactors (Crudo et al. 2016; Samani et al. 2021). As far as our knowledge is concerned, there is no publication about the application of stator-rotor-type hydrodynamic cavitation reactors for intensification of biodiesel production from non-edible castor oil.

Response surface methodology (RSM) based on experimental designs is a time-saving and cost-effective mathematical statistical method for optimizing and studying the main and interactive effects of physicochemical independent variables influencing processes using fewer experimental trials than traditional techniques (Tamilvanan et al. 2016; Nassar et al. 2021). Furthermore, regression analysis may conjecture statistical models that describe the relationship between parameters (independent variables) and process yield (response) for optimization purposes (Nassar et al. 2024).

This study is one of the first to use a self-made cylindrical rotor–stator hydrodynamic cavitation reactor to intensify biodiesel production from the non-edible castor oil feedstock. RSM based on the one-factor at-a-time technique will be applied to statistically investigate and optimize various physicochemical parameters influencing transesterification efficiency. Additionally, regression analysis will be performed to model mathematical correlations that describe the effect of the studied physicochemical parameters on the transesterification efficiency, especially the biodiesel yield and the decrease in viscosity, density, and TAN. In a forerunning step, the kinetics and thermodynamics of the process will be investigated under the predicted optimized conditions. The qualification of the produced biodiesel and different bio-/petro-diesel blends will also be evaluated.

Materials and methods

Experimental set-up

A 190-mL rotor–stator hydrodynamic cavitation reactor with a working capacity of 75 mL was used in this study for a

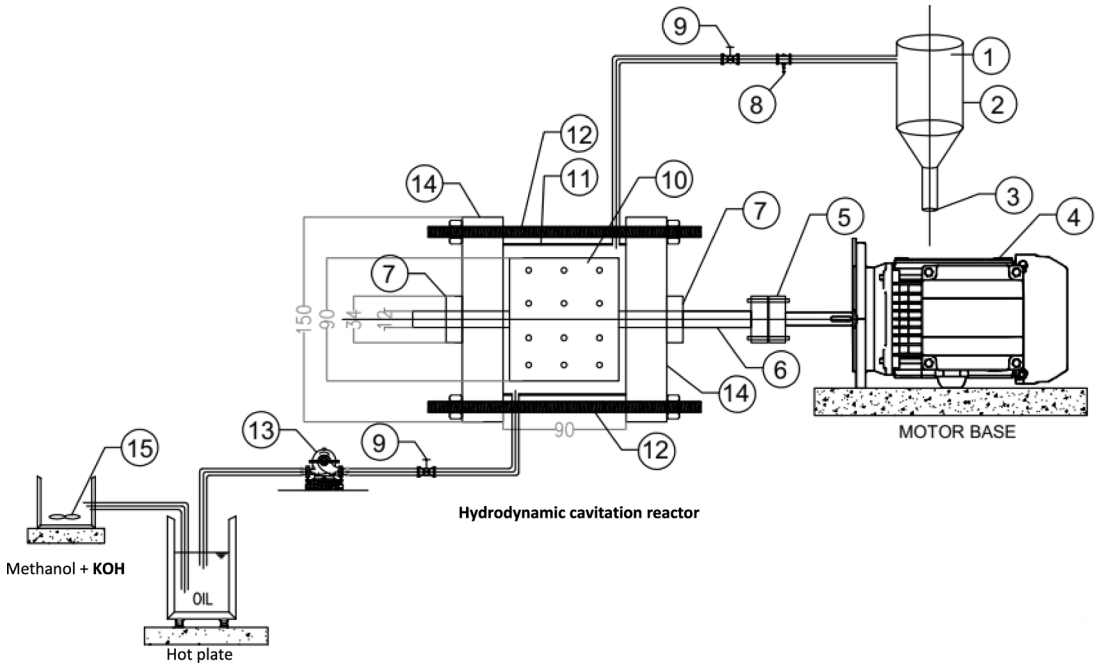

No.	Description	No.	Description	No.	Description
1	Biodiesel	6	Mechanical stainless steel shaft	11	Hollow cylindrical stator
2	Separating funnel	7	High speed bearing	12	8 mm threaded bolt with nuts
3	Glycerol	8	Sampling point	13	Peristaltic pump
4	Electric motor (3000 rpm)	9	Gate valve (isolation)	14	Flange
5	Flexible shaft coupling	10	Cylindrical rotor	15	Magnetic stirrer

Fig. 1 Schematic diagram of the process

one-step alkaline transesterification process of castor oil. Figure 1 shows the schematic diagram of the hydrodynamic cavitation reactor. It consists mainly of two parts: the reactor and the motor, which is responsible for the rotor's rotation. This motor has power of 0.37 KW and it is connected to a shaft made of stainless steel (316). The reactor consists of parts including the stator, which is a hollow cylinder made of polycarbonate material, and the rotor, which is a solid cylinder, made of Acrylonitrile Butadiene Styrene (ABS) as shown in Table 1. The gap between the stator and rotor was 7 mm, and the inlet pressure was 1 bar. Circular cavities were perforated in the rotor surface, whose centers were placed at 45-degree angles from one another, originating from the center line of the rotor.

The utilized castor oil in this study has a viscosity of 192.8 cSt, a density of 0.9594 g/cm^3, and a total acid number (TAN) of 1.2 mg KOH/g oil. Potassium methoxide (CH_3OK) was formed by mixing methanol with KOH of a particular weight. The oil was then mixed with CH_3OK after it attained the desired temperature. The process was carried out under atmospheric pressure.

Table 1 Characteristics of the hydrodynamic cavitation reactor

Parameter	Value
Rotor diameter (mm)	90
Rotor length (mm)	80
Stator diameter (mm)	97
Stator length (mm)	90
Rotor density (g/cm^3)	2.3
Cavity diameter (mm)	4
Cavity depth (mm)	6
Number of cavities	64
Electric-motor power (KW)	0.37
Electric-motor rotational speed (rpm)	3000

Following the specified reaction time, the mixture was cooled down, collected from the reactor outlet and then moved to a separating funnel, where the biodiesel was separated from the glycerol in the bottom layer (Fig. 1). In order to separate the mixture efficiently, 120 min was allotted for settling separation. After the separation of glycerol, the unreacted dissolved KOH catalyst was removed from the

produced biodiesel by rinsing with warm water. A rotary evaporator set at 65 °C was then used to recover the unreacted methanol from biodiesel. Then, the weight of the purified biodiesel was determined for yield computations using the following equation:

$$Biodieselyield\% = \frac{weightofpurifiedbiodiesel}{weightofcastoroilfeedstock} \times 100 \quad (1)$$

Fuel ageing is influenced by the acid value, which quantifies the amount of free acids present in the sample (El-Gendy et al., 2014). The viscosity at 40 °C and density at 15 °C are important parameters, notably in airless combustion systems, since they determine the effectiveness of atomization of the fuel, its distribution, and flow (Felizardo et al. 2006). Thus, the viscosity, density, and TAN of the oil feedstock and the biodiesel produced at different prescribed time intervals were also measured according to the ASTM D-445, ASTM D-4052, and ASTM D-974, respectively. Then, the percentage decrease was calculated as follows:

$$Viscositydecrease\% = \frac{V_o - V_t}{V_o} \times 100 \quad (2)$$

$$Densitydecrease\% = \frac{\rho_o - \rho_t}{\rho_t} \quad (3)$$

$$TAN = \frac{TAN_o - TAN_t}{TAN_o} \times 100 \quad (4)$$

where V_o, ρ_o, and TAN_o are the initial castor oil feedstock viscosity, density and total acid number, respectively. The V_t, ρ_t, and TAN_t are the viscosity, density and total acid number of the produced biodiesel at time (t), respectively.

According to Attia et al. (2018), it is preferred to determine the free fatty acid (FFA) content of the feedstock to decide whether to perform a two-step process (esterification followed by transesterification) or a direct one-step process (i.e., transesterification). The FFA content was calculated as follows (Attia et al. 2018):

$$FFA\% = \frac{TAN}{1.99} \quad (5)$$

Accordingly, the FFA content of the used castor oil was 0.603%, which is < 3%. Thus, a single-step transesterification process is applied in this study.

Experimental design

Response surface methodology (RSM) is a collection of mathematical techniques for evaluating relationships between responses and variables, modelling, and minimizing the number of experiments required (El-Gendy et al., 2014). RSM based on a one-factor-at-a-time (OFAT) experiment was applied to study the effects of five independent variables on the biodiesel yield and the decrease in viscosity, density, and TAN. In this study, the independent variables were temperature (40–70 °C), KOH catalyst concentration (0.5–1.5 wt.%), M:O molar ratio (6:1–12:1), rotor-rotational speed (1000–2000 rpm), and time (2–60 min). They were denoted as A, B, C, D, and E, respectively. In accordance, 32 runs were performed, as listed in Table 2. All the trials were performed in triplicate, and the arithmetic means of the obtained responses were employed for the interpretation of the data and modelling. A Tukey-test, applying SPSS-software version 13.0 (Informer Technologies, Inc., Los Angeles, CA, USA), was used to assess the significance difference between levels in each studied parameter at the 0.05 level and 95% confidence interval.

Modelling and statistical analysis

The general quartic equation used for model development is shown in Eq. 6.

$$Y = b_o + \sum_{i=1}^{n} b_i x_i + \sum_{i=1}^{n} c_{ii} x_i^2 + \sum_{i=1}^{n-1} \sum_{j>1}^{n} c_{ij} x_i x_j \sum_{i=1}^{n} d_{ii} x_i^3 + \sum_{i=1}^{n} e_{ii} x_i^4 + \varepsilon \quad (6)$$

The model coefficient constant is b_o, and the coefficients for the intercept of linear, quadratic, interactive, cubic, and quartic terms are b_i, c_{ii}, c_{ij}, di_i, and e_{ii}, respectively. X_i and X_j denote the independent variables ($i \neq j$), while Y represents the predictive response. The independent variable numbers are represented by n along with ε, the random error. For the predicted models, the adequacies were examined using different statistical analytical methods that include adequacy precision, correlation coefficient (R^2), and adjusted coefficient of determination (R^2_{adj}). Furthermore, Fisher's test, i.e., F-value and p-value, at a 95% confidence interval and analysis of variance (ANOVA) were used to check the statistical significance of the predicted models. In addition to investigating the fitting accuracy of the predicted models to the experimental data, a lack of fit analysis was employed. For design of experiments, regression analysis, graphical analysis, and numerical optimization, design expert software version 14 (Stat-Ease Inc., Minneapolis, MN, USA) was used.

Table 2 Experimental design matrix with the actual and predicted responses

Run	Temp. (°C)	Cat. Conc. (wt.%)	M:O ratio	Rotational speed (rpm)	Time (h)	Actual BD yield (%)	Predicted BD Yield (%)	Actual viscosity decrease (%)	Predicted viscosity decrease (%)	Actual density decrease (%)	Predicted density decrease (%)	Actual TAN decrease (%)	Predicted TAN decrease (%)
1	50	0.75	8	1500	20	94.21	93.61	94.34	94.28	4.96	4.78	83.33	78.59
2	60	0.75	8	1500	20	87.12	87.16	91.45	91.72	4.10	3.79	60.33	64.41
3	50	0.75	8	1750	20	92.00	92.00	91.45	91.45	3.15	3.15	76.67	76.67
4	50	0.75	8	1500	20	94.21	93.61	94.34	94.28	4.96	4.78	83.40	78.59
5	50	0.75	8	1500	4	79.61	80.30	91.25	91.11	3.25	3.06	60.00	59.97
6	50	0.75	8	1500	15	92.30	91.14	93.44	93.72	4.03	4.44	66.67	69.67
7	50	0.75	8	1000	20	77.90	77.90	91.63	91.63	3.29	3.29	41.67	41.67
8	70	0.75	8	1500	20	84.01	84.10	90.06	90.12	2.88	2.84	53.00	53.12
9	45	0.75	8	1500	20	88.31	90.86	94.32	93.91	4.91	4.73	66.67	72.56
10	50	0.75	8	1500	5	82.96	81.65	91.88	91.44	3.28	3.23	59.00	59.43
11	50	0.5	8	1500	20	84.29	84.29	92.17	92.21	3.29	3.34	58.3	58.33
12	50	0.75	6	1500	20	81.09	81.09	91.58	91.58	3.30	3.30	50.00	50.00
13	50	1	8	1500	20	90.18	90.18	93.3	93.56	3.96	4.27	75.00	75.00
14	50	0.75	8	1500	20	94.21	93.61	94.34	94.28	4.96	4.78	83.00	78.59
15	50	0.75	8	1500	40	94.52	94.75	94.30	94.34	4.97	5.07	88.00	87.91
16	50	0.75	8	1500	20	94.21	93.61	94.34	94.28	4.96	4.78	83.10	78.59
17	50	0.75	8	1500	30	94.93	95.39	94.33	94.60	4.96	5.09	85.19	86.91
18	50	0.75	8	1500	2	76.88	77.36	90.02	90.38	2.74	2.71	59.00	60
19	50	0.75	8	1500	50	94.63	94.88	94.33	94.09	4.96	4.95	88.33	89.96
20	50	0.75	8	2000	20	90.8	90.80	90.96	90.96	3.00	3.00	75.00	75.00
21	50	0.75	8	1500	10	86.81	87.24	92.58	92.80	3.46	3.93	61.56	61.97
22	40	0.75	8	1500	20	80.9	80.25	91.25	91.37	3.96	4.01	52.00	50.21
23	50	1.25	8	1500	20	89.74	89.74	92.36	92.19	3.51	3.30	66.67	66.67
24	50	1.5	8	1500	20	89.41	89.41	92.27	92.31	3.35	3.40	66.52	66.60
25	50	0.75	10	1500	20	91.6	91.60	93.26	93.26	4.04	4.04	75.00	75.00
26	50	0.75	8	1500	25	94.97	94.94	94.31	94.55	4.95	4.99	84.33	85.92
27	50	0.75	8	1500	60	94.67	94.97	94.35	94.45	4.98	4.96	88.30	89.82
28	55	0.75	8	1500	20	89.42	91.42	93.67	93.28	4.27	4.40	75.00	73.98
29	50	0.75	8	1250	20	85.4	85.40	91.68	91.68	3.22	3.22	58.33	58.33
30	65	0.75	8	1500	20	84.15	83.76	90.58	90.39	3.01	3.20	57.33	55.56
31	50	0.75	8	1500	20	94.21	93.61	94.34	94.28	4.96	4.78	83.33	78.59
32	50	0.75	12	1500	20	90.18	90.18	92.33	92.33	3.94	3.94	66.67	66.67

Reaction kinetics

The rate equation for the generation of FAME in the transesterification process can be expressed by Eq. 7;

$$r = -\frac{d[TG]}{dt} = k_1[TG]^{\alpha}[MeOH]^{\beta} - k_2[GL]^{\lambda}[FAME]^{\mu} \quad (7)$$

The symbols [TG], [MeOH], [GL], and [FAME] denote the concentrations of triglycerides, methanol, glycerol, and fatty acid methyl esters, respectively. α, β, λ, and μ represent the reaction order coefficients for the concentrations of triglycerides, methanol, glycerol, and fatty acid methyl esters, respectively. Additionally, k_1 and k_2 denote the response rate constants for the forward and backward reactions, respectively.

$$r = -\frac{d[TG]}{dt} = k_1[TG]^{\alpha} \quad (8)$$

$$\frac{d[TG]}{[TG]} = -k_1 dt \quad (9)$$

Assuming the reaction is irreversible and that the concentration of methanol remains constant due to its excess use, the reaction rate equations (Eqs. 8 and 9) exclude the backward reaction rate and the methanol concentration.

To calculate the conversion without evaluating the final concentration of the triglycerides, it is necessary to take into account the fact that the molecular weight of the TG is three times that of FAME, as stated in Eq. 10;

$$X = \frac{[FAME]}{3[TG]_o} = \frac{m_{FAME}/M_{FAME}}{3m_{TG_o}/M_{TG}} = \frac{m_{FAME}/3M_{FAME}}{m_{TG_o}/M_{TG}} = \frac{m_{FAME}}{m_{TG_o}} = Y \quad (10)$$

The term "FAME" refers to the concentration of fatty acid methyl esters. The "m_{FAME}" represents the mass of FAME, while the "M_{FAME}" represents the molecular mass of FAME. Y represents the yield of FAME, whereas X represents the conversion of TG.

Physico–chemical characterization of produced biodiesel and bio-/petro-diesel blends

The physico-chemical properties of the produced biodiesel were tested according to the American Standard Test Methods (ASTM). The results were compared with the international biodiesel standards (EN14214 and ASTM-D6751). On a volume basis, blends of bio- and petro-diesel were prepared, and their physico-chemical characteristics were also evaluated relative to the international standard (ASTM-D7467).

Results and discussion

Regression model development

A set of 32 random experimental runs (Table 2), were conducted to assess the biodiesel yield, reduction in viscosity, density, and TAN. These responses are denoted as Y_1, Y_2, Y_3, and Y_4, respectively, and ranged from 76.88% to 94.97%, 90.02% to 94.35%, 2.74% to 4.98%, and 41.67% to 88.33%, respectively (Table 2).

The correlation between the studied parameters and experimental results was tested to be represented by linear, two-factor interactions (2FI), quadratic, cubic, and quartic polynomials. The software indicated that the most appropriate model was the quartic regression model. Thus, four quartic models have been generated to represent the reactions of process variables;

$$\begin{aligned} Y_1 = {} & 89.46 - 11.05A - 6.02B - 3.97C + 6.65D + 0.0571E - 11.91A^2 + 9.10\,B^2 - 7.85C^2 \\ & - 23.14D^2 - 5.19E^2 + 12.97A^3 + 8.58B^3 + 8.52C^3 - 0.2D^3 + 8.83E^3 + 2.54A^4 - 12.43B^4 \\ & + 13.86D^4 - 3.96E^4 \end{aligned} \quad (11)$$

$$\begin{aligned} Y_2 = {} & 92.08 - 4.29A - 2.59B - 1.78C - 0.195D - 0.33E - 1.55A^2 + 0.492B^2 - 2.05C^2 - 13.53D^2 \\ & - 1.02E^2 + 3.68A^3 + 2.64B^3 + 2.16C^3 - 0.14D^3 + 2.39E^3 - 0.951A^4 - 1.57B^4 + 10.54D^4 - 1.14E^4 \end{aligned} \quad (12)$$

$$\begin{aligned} Y_3 = {} & 3.67 - 1.64A - 1.74B - 1.33C - 0.045D + 0.145E - 0.821A^2 + 1.27B^2 - 0.904C^2 - 8.09D^2 \\ & - 2.20E^2 + 1.05A^3 + 1.77B^3 + 1.65C^3 - 0.1D^3 + 0.968E^3 - 0.158A^4 - 1.91B^4 + 6.43D^4 + 0.902E^4 \end{aligned} \quad (13)$$

Table 3 Analysis of variance of the developed models Eq. 11 and Eq. 12

Biodiesel yield developed model Eq. 11							Decrease in viscosity developed model Eq. 12					
	Sum of squares	df	Mean Square	*F*-value	*p*-value	Significance*	Sum of Squares	df	Mean Square	*F*-value	*p*-value	Significance*
Model	931.74	19	49.04	37.03	< 0.0001	VHS	64.32	19	3.39	42.81	< 0.0001	VHS
A- Temperature	77.44	1	77.44	58.47	< 0.0001	VHS	11.70	1	11.70	147.89	< 0.0001	VHS
B- Cat conc	17.86	1	17.86	13.48	0.0032	S	3.30	1	3.30	41.73	< 0.0001	VHS
C- M:O molar ratio	4.97	1	4.97	3.76	0.0765	NS	1.00	1	1.00	12.68	0.0039	S
D- Rotational speed	12.25	1	12.25	9.25	0.0103	PS	0.0105	1	0.0105	0.1332	0.7215	NS
E-Time	0.0022	1	0.0022	0.0017	0.9680	NS	0.0745	1	0.0745	0.9426	0.3508	NS
A^2	8.51	1	8.51	6.42	0.0262	PS	0.1436	1	0.1436	1.82	0.2027	NS
B^2	2.51	1	2.51	1.90	0.1934	NS	0.0073	1	0.0073	0.0928	0.7658	NS
C^2	62.52	1	62.52	47.21	< 0.0001	VHS	4.26	1	4.26	53.83	< 0.0001	VHS
D^2	31.37	1	31.37	23.68	0.0004	HS	10.73	1	10.73	135.69	< 0.0001	VHS
E^2	2.15	1	2.15	1.62	0.2267	NS	0.0828	1	0.0828	1.05	0.3264	NS
A^3	68.70	1	68.70	51.87	< 0.0001	VHS	5.52	1	5.52	69.79	< 0.0001	VHS
B^3	25.71	1	25.71	19.42	0.0009	HS	2.43	1	2.43	30.75	0.0001	HS
C^3	19.10	1	19.10	14.42	0.0025	S	1.23	1	1.23	15.52	0.0020	S
D^3	0.0090	1	0.0090	0.0068	0.9357	NS	0.0044	1	0.0044	0.0558	0.8173	NS
E^3	34.98	1	34.98	26.42	0.0002	HS	2.56	1	2.56	32.31	0.0001	HS
A^4	0.4509	1	0.4509	0.3404	0.5704	NS	0.0631	1	0.0631	0.7976	0.3894	NS
B^4	6.23	1	6.23	4.71	0.0508	NS	0.0997	1	0.0997	1.26	0.2836	NS
D^4	11.39	1	11.39	8.60	0.0126	PS	6.57	1	6.57	83.11	< 0.0001	VHS
E^4	1.38	1	1.38	1.04	0.3279	NS	0.1138	1	0.1138	1.44	0.2534	NS

**P*-values < 0.05 indicate the model terms are significant. *P*-values > 0.1 indicate the model terms are not significant. S, significant; PS, possibly significant; HS, highly significant; VHS, very highly significant; NS, not significant

Table 4 Analysis of variance of the developed models Eq. 13 and Eq. 14

Decrease in density developed model Eq. 13							TAN conversion developed model Eq. 14					
	Sum of square	df	Mean Square	*F*-value	*p*-value	Significance*	Sum of Squares	df	Mean Square	*F*-value	*p*-value	Significance*
Model	19.14	19	1.01	16.84	< 0.0001	VHS	4608.43	19	242.55	6.96	0.0007	HS
A-Temperature	1.70	1	1.70	28.39	0.0002	HS	359.53	1	359.53	10.32	0.0075	S
B- Cat conc	1.49	1	1.49	24.87	0.0003	HS	148.48	1	148.48	4.26	0.0613	NS
C- M:O molar ratio	0.5601	1	0.5601	9.36	0.0099	S	16.37	1	16.37	0.4700	0.5060	NS
D- Rotational speed	0.0006	1	0.0006	0.0094	0.9245	NS	8.58	1	8.58	6.2462	0.0287	PS
E-Time	0.0143	1	0.0143	0.2389	0.6338	NS	38.29	1	38.29	1.10	0.3151	NS
A^2	0.0404	1	0.0404	0.6762	0.4269	NS	75.77	1	75.77	2.18	0.1660	NS
B^2	0.0490	1	0.0490	0.8183	0.3835	NS	2.09	1	2.09	0.0601	0.8105	NS
C^2	0.8293	1	0.8293	13.86	0.0029	S	439.59	1	439.59	12.62	0.0040	S
D^2	3.84	1	3.84	64.16	< 0.0001	VHS	369.22	1	369.22	10.60	0.0069	S
E^2	0.3872	1	0.3872	6.47	0.0257	PS	354.90	1	354.90	10.19	0.0077	S
A^3	0.4535	1	0.4535	7.58	0.0175	PS	260.33	1	260.33	7.47	0.0181	PS
B^3	1.09	1	1.09	18.25	0.0011	S	161.92	1	161.92	4.65	0.0521	PS
C^3	0.7196	1	0.7196	12.03	0.0046	S	63.60	1	63.60	1.83	0.2015	NS
D^3	0.0023	1	0.0023	0.0376	0.8495	NS	27.72	1	27.72	0.7959	0.3899	NS
E^3	0.4203	1	0.4203	7.03	0.0211	PS	17.34	1	17.34	0.4979	0.4939	NS
A^4	0.0017	1	0.0017	0.0292	0.8673	NS	11.02	1	11.02	0.3164	0.5842	NS
B^4	0.1472	1	0.1472	2.46	0.1427	NS	0.7103	1	0.7103	0.0204	0.8888	NS
D^4	2.45	1	2.45	40.93	< 0.0001	VHS	206.46	1	206.46	5.93	0.0315	PS
E^4	0.0716	1	0.0716	1.20	0.2955	NS	242.04	1	242.04	6.95	0.0217	PS

**P*-values < 0.05 indicate the model terms are significant. *P*-values > 0.1 indicate the model terms are not significant. *S, significant; PS, possibly significant; HS, highly significant;; VHS, very highly significant; NS, not significant

$$Y_4 = 83.96 - 23.81A - 17.37B - 7.21C + 5.56D + 7.49E - 35.54A^2 - 8.30B^2 - 20.80C^2 - 79.385D^2 - 66.67E^2 + 25.24A^3 + 21.54B^3 + 15.54C^3 + 11.1D^3 + 6.22E^3 + 12.57A^4 - 4.20B^4 + 59.06D^4 + 52.44E^4 \quad (14)$$

The independent variables are represented by A, B, C, D, and E, which correspond to temperature (°C), catalyst concentration (wt.%), M:O molar ratio, stirring rate (rpm), and reaction time (min), respectively. In addition, A^2–A^4, B^2–B^4, C^2–C^4, D^2–D^4, and E^2–E^4 denote the surpluses of each individual variable. According to the coefficients in Eqs. (11–14) the reaction temperature and catalyst concentration express the highest effect on the transesterification process and all of the studied responses, followed by the M:O molar ratio and the stirring rate. The positive and

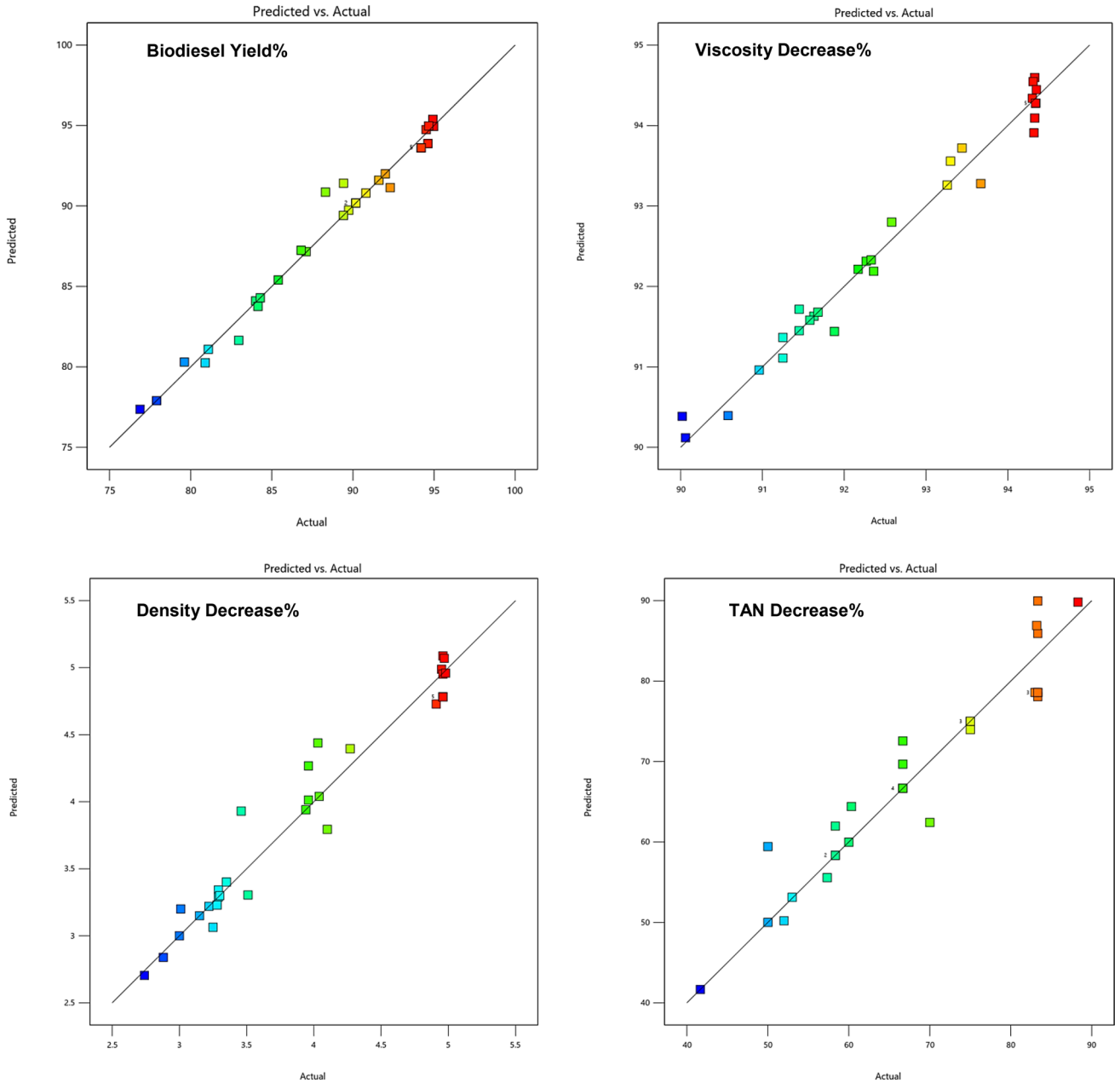

Fig. 2 Actual versus predicted responses

negative signs on each variable coefficient indicate the synergistic and antagonistic influences on the response.

Statistical adequacy checking

ANOVA is useful for assessing the constructed model and determining the impact of parameters. This was determined by evaluating the *F*-value and p-value of each model. The *F*-vales ranged between 6.96 and 42.81 (Tables 3 and 4), implying that the models are significant. Thus, for model Eqs. 11, 12, and 13, there is only a 0.01% chance that an F-value this large could occur due to noise. However, for model Eq. 14, there is only a 0.07% chance that an *F*-value this large could occur due to noise. The *P*-values for the created models representing the effect of process parameters on the biodiesel yield, decrease in viscosity, density, and TAN are less than 0.001 (Tables 3 and 4). That indicates, according to El-Gendy et al. (2014), a high level of statistical significance. The recorded R^2 and R^2_{adj} values were 0.90 and 0.81 for the biodiesel yield, 0.92 and 0.85 for the decrease in viscosity, 95.28 and 90.24 for the decrease in density,

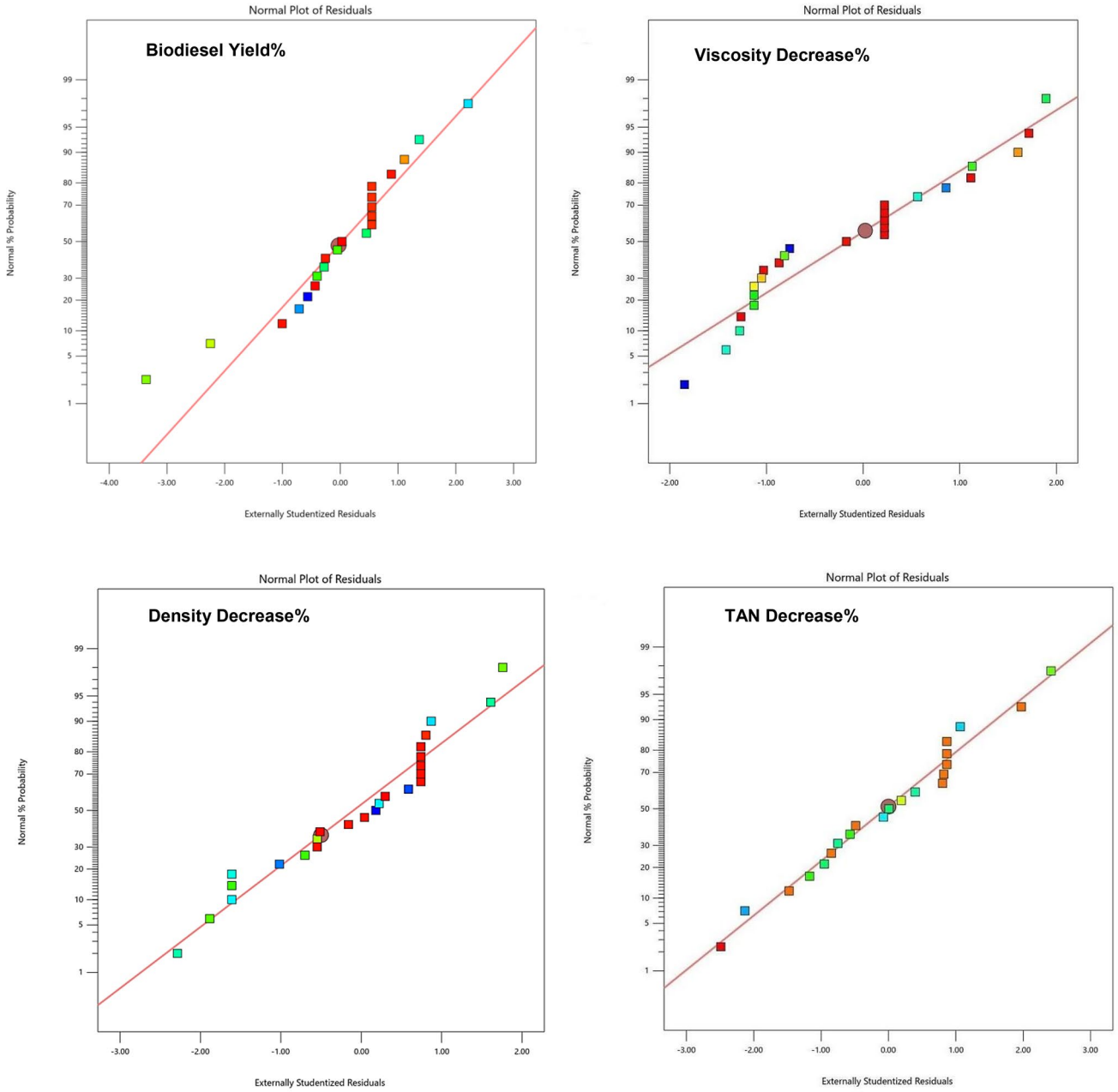

Fig. 3 Normal probability plots of the externally studentized residuals

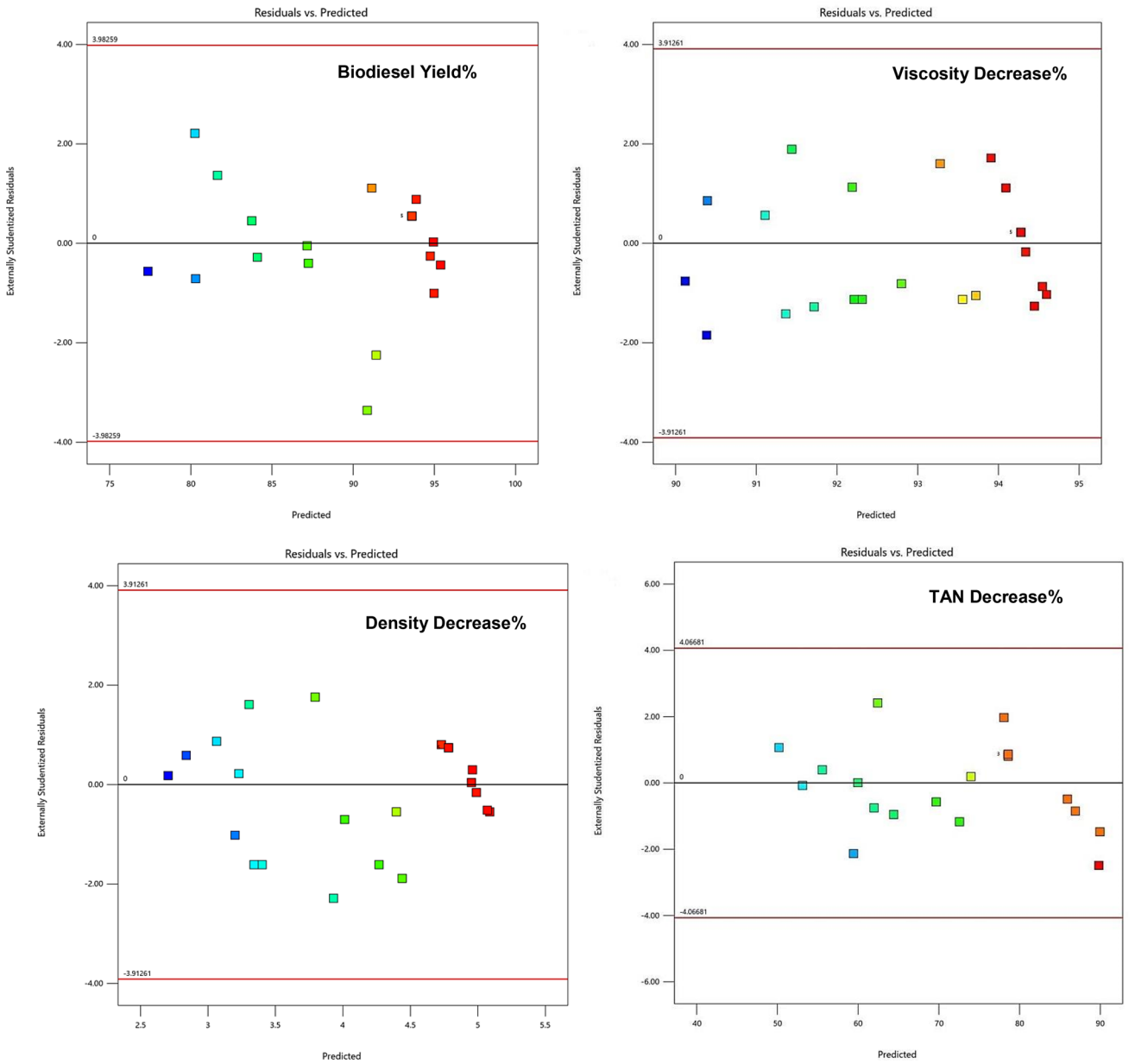

Fig. 4 Diagnostic plots for the externally studentized residuals vs. predicted responses

and 91.47 and 82.65 for the decrease in TAN, respectively. That, according to Ismail et al. (2017), indicates the good fit of the data. Further, the adequate precision test, which measures the ratio between the expected response and the relative error (signal-to-noise ratio) has been evaluated. The test yielded values of 21.35, 21.46, 15.55, and 14.94 for biodiesel yield, decrease in viscosity, density, and TAN, respectively. Typically, a value greater than 4 is desirable, and signifying the reproducibility and accurateness of the anticipated models (Nassar et al. 2021).

Figure 2 displays the graphs comparing the experimental findings with the anticipated outcomes of the models and shows a very slight deviation from the 45-degree line. That confirmed the good agreement between the experimental and predicted values, and consequently, the appropriateness of the predicted regression model Eqs. (11–14).

Three assumptions of ANOVA have been assessed to verify the validity of the anticipated models. These assumptions include externally studentized residuals, normality of residuals, and randomization. The quotient obtained by dividing the residual of an estimate by its standard deviation represents the externally studentized residual. The normality of the residuals has been examined and appears to follow a linear pattern, as seen in Fig. 3. The randomization has

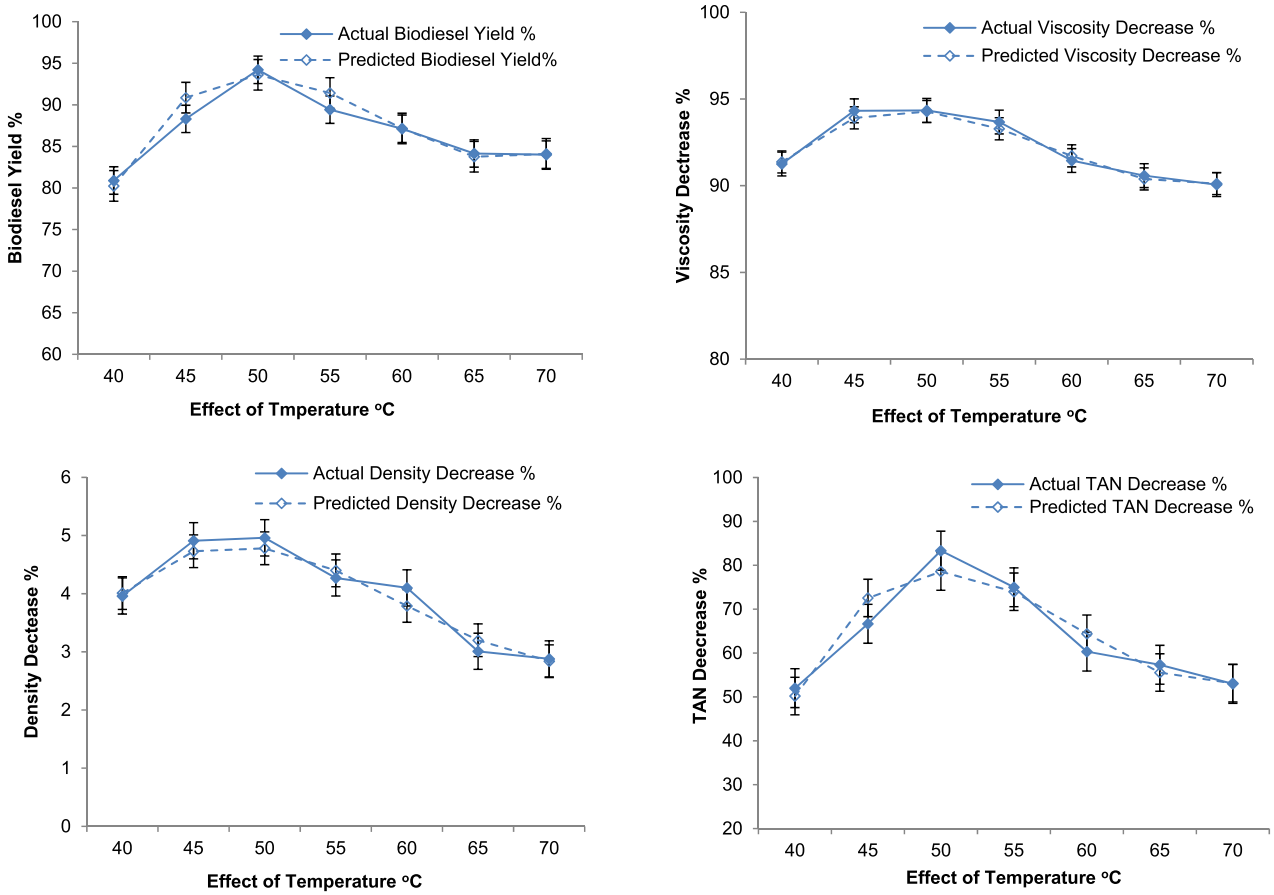

Fig. 5 Effect of temperature on different responses

been assessed by analyzing the residuals plotted against the anticipated response value. Figure 4 demonstrates that the residuals exhibited a random spread between ±4 without any discernible pattern. Thus, all the tested three ANOVA assumptions verify the validity of the predicted quartic regression models.

Impact of process variables

The impact of reaction temperature

The ANOVA analysis reveals that temperature does have a statistically significant impact on the transesterification process and all the studied responses (Tables 3 and 4). The study focused on the temperature range of 40–70 °C due to the fact that the boiling point of methanol is 65 °C. It is shown in Fig. 5 that the temperature has a positive impact on all responses from 40 to 50 °C, and the opposite occurs beyond 50 °C. Asif et al. (2021a) attribute the occurrence of this phenomenon to the high volatility of methanol at high temperatures. The existence of methanol in the liquid phase at a lower temperature would enhance the reaction in comparison with a high-temperature reaction with a high turnover of methanol vaporization and condensation (María Elena et al. 2022). The increase in temperature up to 50 °C would have decreased the mass transfer limitation and enhanced the triglycerides' solubility in methanol, enriching the contact surface area between the reactants (Gole et al. 2013). The increase in temperature up to the optimum value decreases the oil feedstock viscosity and consequently enhances the formation of cavities, as according to Mohod et al. (2017), the higher the oil viscosity, the lower the occurrence of cavitation. However, the cushioned collapse of a large number of cavities reduces the expected cavitational effects, resulting in lower yields when the temperature is above the optimal point (Mohod et al. 2017).

According to the performed Tukey test, there is a high statistical difference between the biodiesel yield at 50 °C and all other recoded yields at different investigated temperatures ($p < 0.0001$). Same-wise is the reduction in TAN ($p < 0.0001$). However, for the decrease in viscosity and density, there is a high statistical difference between the values recorded at 50 °C and those recorded at other

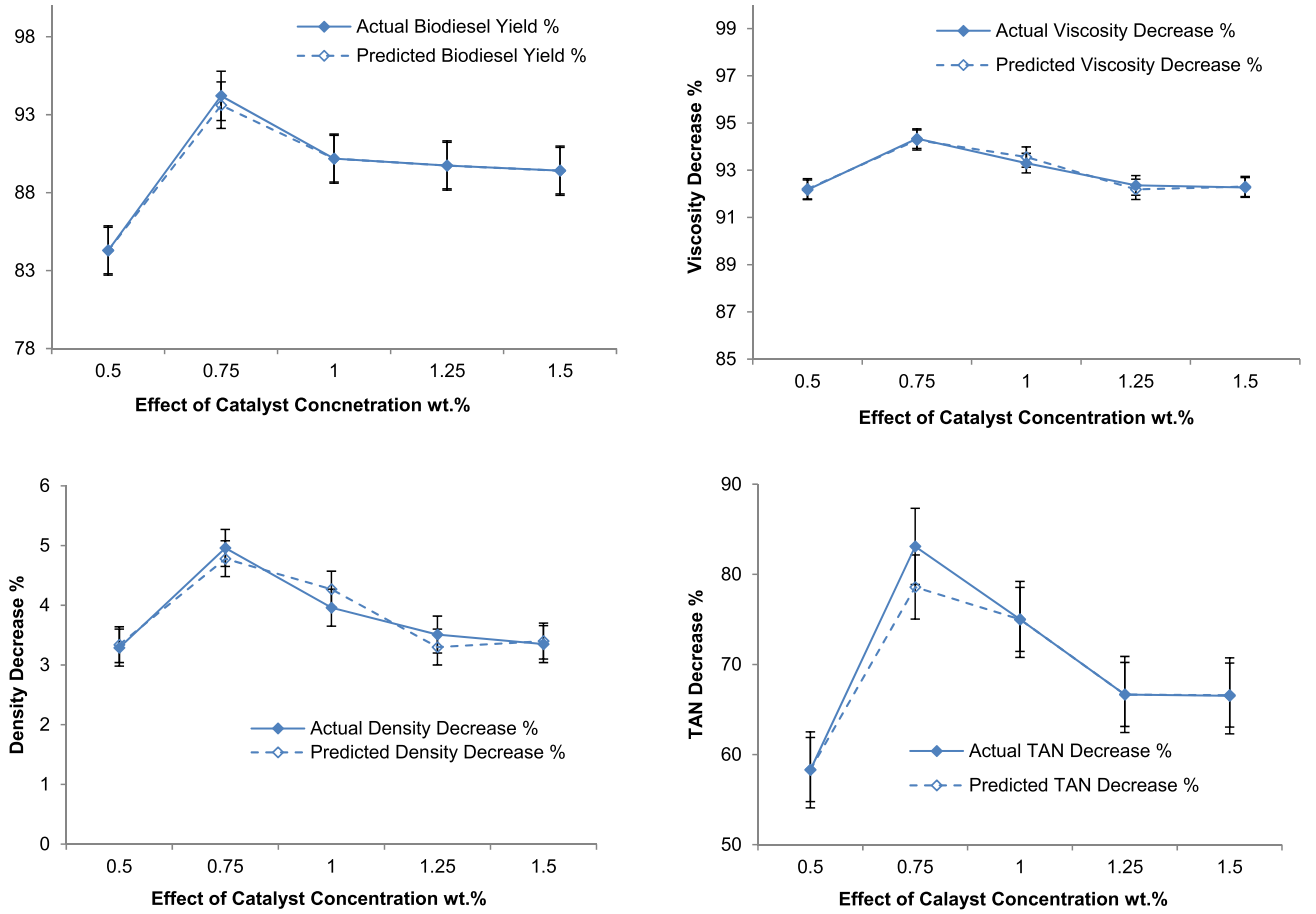

Fig. 6 Effect of catalyst concentration on different responses

reaction temperatures, except for those recorded at 45 °C ($0.983 \leq p \leq 0.999$).

The impact of catalyst concentration

ANOVA demonstrates that the utilized basic homogenous catalyst (KOH) has a statistical substantial impact on the transesterification process and all the studied responses (Tables 3, 4). A higher catalyst dose (> 0.75 wt.%) has a negative impact on the transesterification process and all of the studied responses, resulting in a decrease in biodiesel output (Fig. 6). However, the increase in the catalyst dose from 0.5 to 0.75 wt.% has a positive impact on the transesterification process outputs (Fig. 6). Farvardin et al. (2022) reported a similar observation, attributing it to saponification rather than transesterification at higher KOH concentrations. According to Kolhe et al. (2017), upon employing a hydrodynamic cavitation reactor for biodiesel production, a small amount of basic catalysts is required. That is because the cavitation bubbles are collapsing, which interrupts the phase boundary and results in emulsification, which pushes one liquid against another while compensating for the mass transfer barrier to advance the reaction. According to Mohod et al. (2017), the catalyst is employed to produce the first required active ions in the reaction, and the concentration of the catalyst generally causes a rise in the number of ions. Therefore, decreased catalyst loading below the ideal catalyst concentration (0.75 wt.%) offers insufficient active sites for the reaction to proceed, resulting in lesser triglyceride conversion and, consequently, poorer yields. Nonetheless, the increase in catalyst concentration is not recommendable, as this will increase the water consumption in the biodiesel purification step (Asif et al. 2021a).

The accomplished Tukey test proved that there is a high statistically significant difference between the recorded responses in batches fed with 0.75 wt.% KOH and those fed with other catalyst concentrations ($p < 0.0001$).

Impact of the molar ratio of M:O

The ANOVA analysis reveals that the studied range of M:O molar ratio statistically does not significantly impact the transesterification process (Tables 3, 4). The biodiesel yield

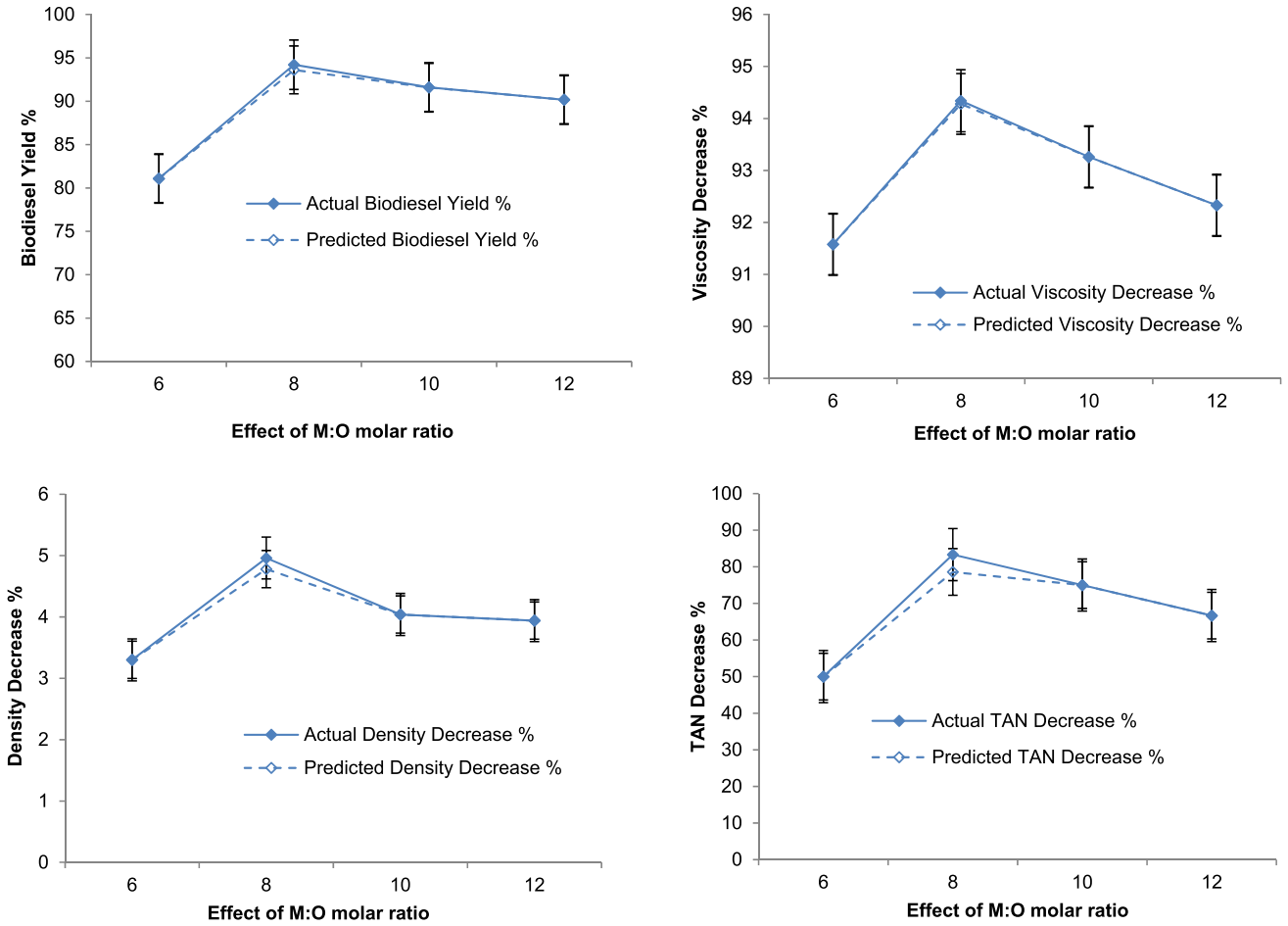

Fig. 7 Effect of M:O molar ratio on different responses

ranged between 81.09% and 90.18% at M:O molar ratios of 6:1 and 12:1, respectively. That occurred with a consequent decrease in viscosity, density, and TAN, which ranged between 91.58% and 92.33%, 3.30% and 3.94%, and 50% and 66.67%, respectively. Thus, a higher methanol ratio has a negligible impact on the yield of biodiesel and is hence considered an insignificant parameter in the ANOVA, and (C^4) was deleted from the predicted model Eqs. (12–15).

However, according to the obtained outputs of the Tukey test, there is a high statistical difference between the recorded responses in batches fed with an 8:1 M:O molar ratio and those fed with other alcohol concentrations ($p < 0.0001$).

Increasing the molar ratio of M:O from 6:1 to 8:1 enhanced the transesterification process and all the investigated responses (Fig. 7). As the ratio has exceeded the stoichiometric ratio of 3:1, it thus enhances the reversible transesterification reaction forward towards biodiesel production (Chuah et al. 2015). According to Khan et al. (2020), the higher the viscosity of the oil feedstock, the higher the required methanol is to boost the oil/alcohol miscibility. But that should be to a certain extent; otherwise, oil dilution would occur, in addition to the occurrence of biodiesel emulsification in the warm-water purification step, with a consequent lowering in the biodiesel yield output (Asif et al. 2021a).

The increase in biodiesel yield up to 8:1 M:O could be explained by the fact that methanol forms more voids than oil does, leading to low mass transfer resistance (Ghayal et al. 2013). Thus, beyond the optimum required M:O molar ratio, much more cavities would occur, causing a cushioned collapse, which would consequently, lessen the overall impacts of cavitation (Mohod et al. 2017). According to Kolhe et al. (2017), excess methanol decreases the separation of esters and glycerol, due to their high solubility in methanol, and consequently decreases the

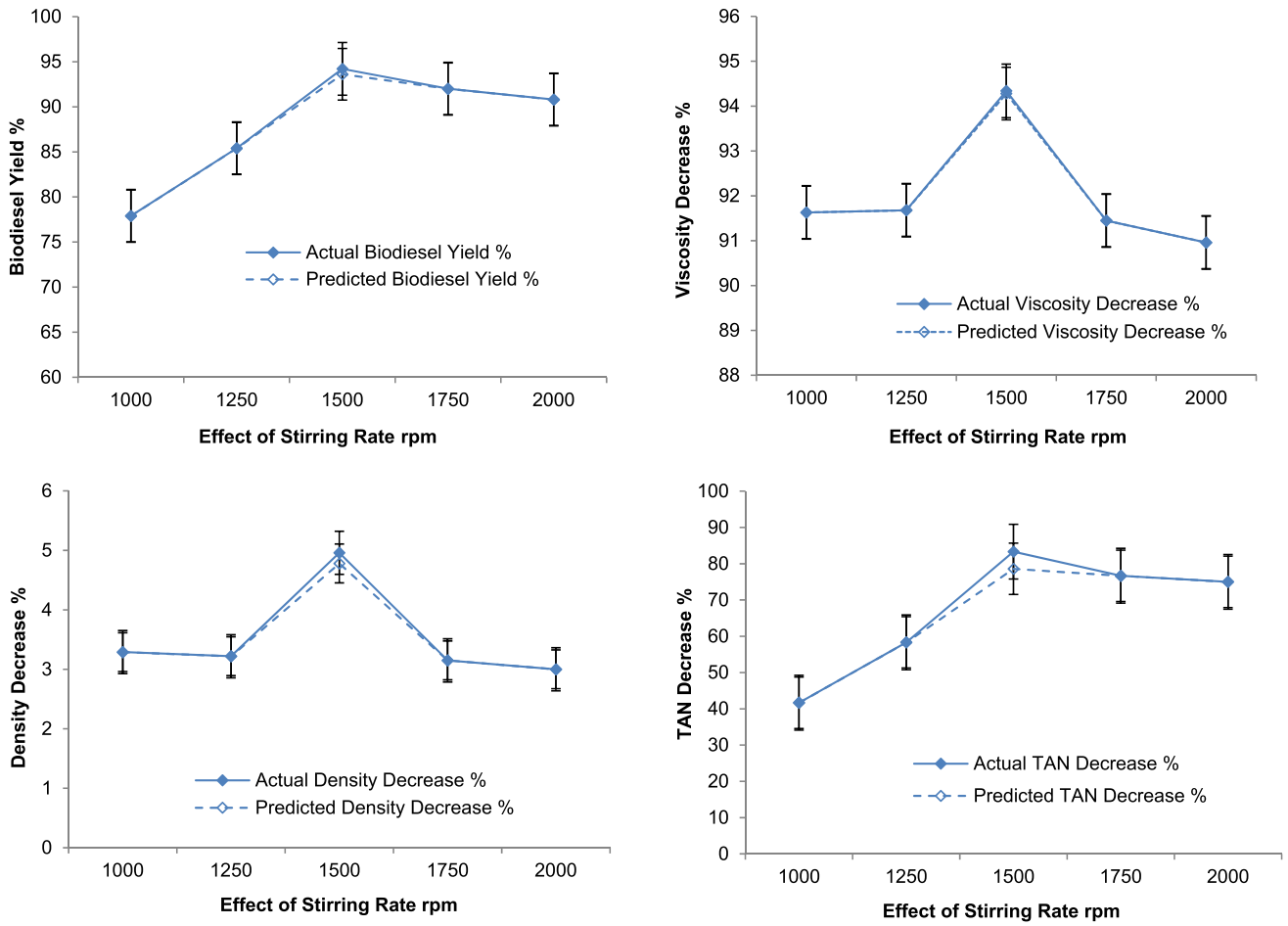

Fig. 8 Effect of rotor- rotational speed on different responses

purified biodiesel yield. Nevertheless, at low methanol concentrations (< 8:1 M:O), part of it would dissolve in the produced glycerol, and the rest would not be enough to fulfil the requirement of complete oil transesterification (Khan et al. 2020). Moreover, methanol prefers reaction with free fatty acids than triglycerides; thus, at low or high methanol concentrations, beyond its required optimum concentration, saponification would occur instead of transesterification, lowering the biodiesel yield output (Gole et al. 2013). The higher the amount of unreacted methanol after the reaction is completed, the higher the methanol recovery cost is (Kolhe et al. 2017).

The impact of the rotational speed

According to the ANOVA results demonstrated in Tables 3 and 4, the investigated rotor-rotational speed range in this study (1000–2000 rpm) has no statistically significant effect on the decrease in viscosity and density of the castor oil feedstock ($0.7215 \le p \le 0.9245$). Those ranged between 91.63% and 90.96%, and 3.29% and 3.00%, respectively. But the investigated rotational speed range in this study (1000–2000 rpm) has been found to have a statistically significant effect on the biodiesel yield ($p = 0.0103$, Table 3) and the decrease in TAN ($p = 0.0287$, Table 4). Those ranged between 77.9% and 90.80%, and 41.67% and 75.00%, respectively.

Based on the performed Tukey test, there is a high statistical difference ($p < 0.0001$) between the obtained responses' values of transesterification batches implemented at 1500 rpm and those fulfilled at other studied rotational speeds.

The increase in rotational speed from 1000 to 1500 rpm has a positive impact on the transesterification process and all the studied responses (Fig. 8). However, at higher rotational speeds (> 1500 rpm), all responses decreased (Fig. 8).

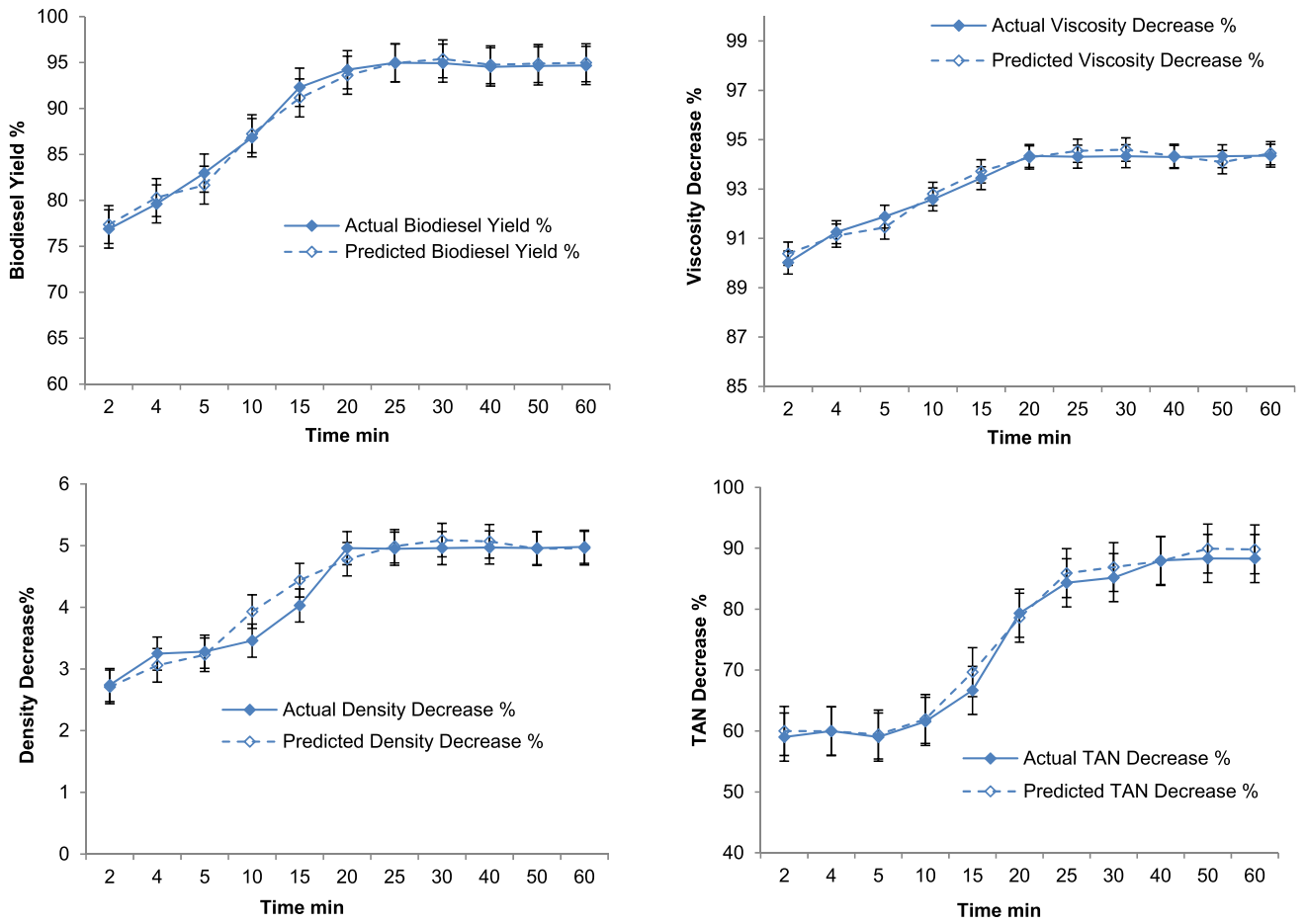

Fig. 9 Effect of time on different responses

Table 5 Optimization constraints to predict the process optimum conditions

Factor	Code	Goal	Importance	Limits	
			Scale 1–5	Lower	Upper
Temperature (°C)	A	in range	–	40	70please remove the dark blue shading from this row
Catalyst conc. (wt.%)	B	in range	–	0.5	1.5
M:O (molar ratio)	C	in range	–	6	12
Stirring speed (rpm)	D	in range	–	1000	2000
Time (min)	E	in range	–	2	60
Biodiesel yield%	Y_1	Maximize	5	76.88	94.97
Viscosity decease%	Y_2	Maximize	5	90.2	94.34
Density decrease%	Y_2	Maximize	5	2.74	4.98
TAN decrease %	Y_2	Maximize	5	41.67	88.33

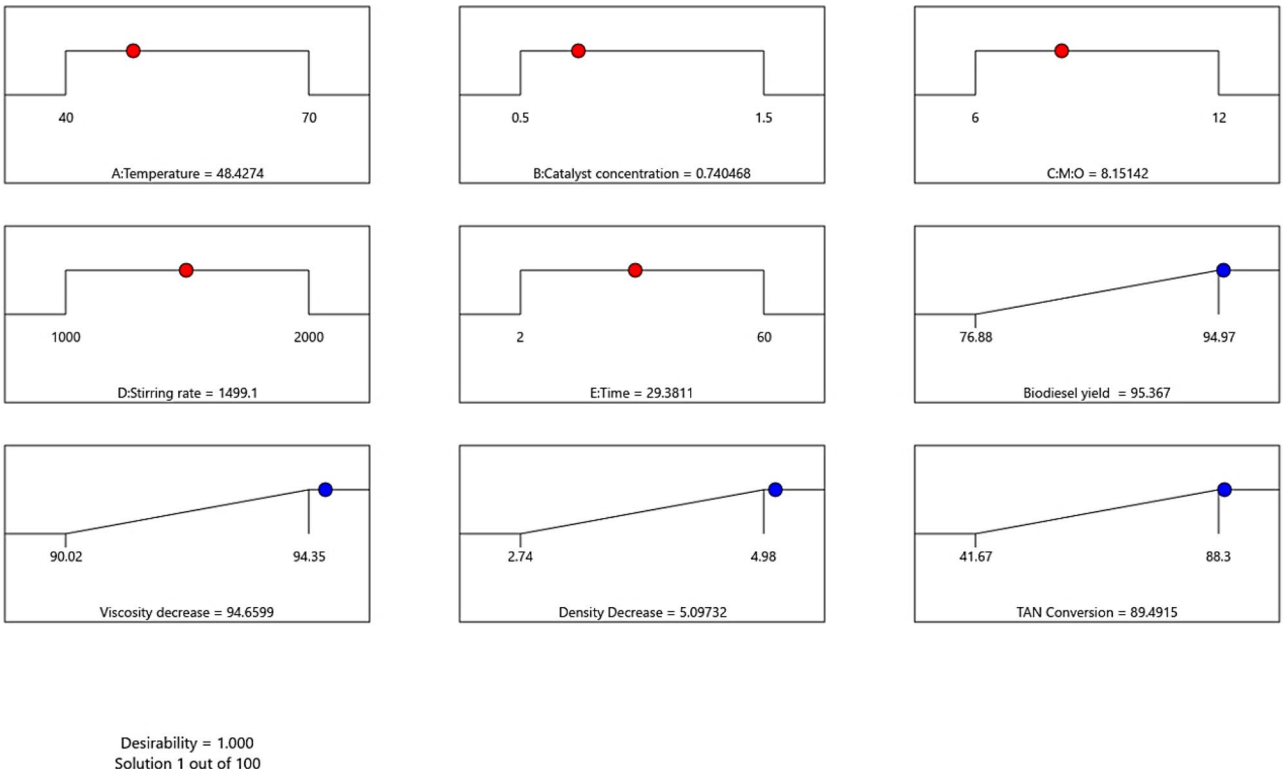

Fig. 10 The optimization ramps

The transesterification reaction takes place at the interface between oil and alcohol. Thus, an increase in rotational speed would overcome the mass transfer resistance and enhance the interaction between reactants (Mohod et al. 2017). Moreover, the cavitation operation would increase with the hydrodynamic reactor's rotational speed, which would raise the conversion rate as well. On the contrary, at a higher rotational rate, an increase in the volatility of methanol would occur and hence impact the M:O molar ratio. Further, the increment of the rotational speed beyond the optimal value results in supercavitation development. That in turn produces the cushioned collapse phenomenon and lessens the overall impacts of cavitation, ultimately lowering the yield of biodiesel and other studied responses (Naderloo 2020).

The impact of reaction time

The ANOVA analysis indicates that the reaction time has an overall non-statistically significant impact on the transesterification process, the biodiesel output, and other studied responses (Tables 3 and 4). However, there is a recorded significant continual increase in biodiesel yield, with a consequent decrease in castor oil feedstock viscosity, density, and TAN up to approximately 20 min (Fig. 9). After which it reached a plateau and remained rather constant (Fig. 9). Thus, it can be depicted that approximately 20 min is the satisfactory amount of time needed for the reactor to diminish the mass transfer obstacle. According to Samuel et al. (2019), the required time for maximum biodiesel production in hydrodynamic reactors differs according to the oil feedstock type and the reactor configuration. According to the quartic model (Eq. 14), the reaction time has a positive effect on the decrease in TAN (i.e., the conversion %), confirming the importance of reaching the optimum residence time to assure the conversion of castor oil into biodiesel.

The Tukey test assured that there is no statistically significant difference for all of the recoded responses' at reaction time $\geq$ 20 min.

Process optimization

Optimizing reaction variables is crucial for achieving effective and highly efficient processes while also considering production and economic costs. Considering the efficiency of process responses, such as biodiesel yield and

Table 6 Comparison of biodiesel yields obtained using various hydrodynamic reactors

Feedstock	Reactor type	M:O molar ratio	Catalyst	Catalyst concentration wt.%	Reaction time min	Temperature °C	Biodiesel yield%	References
Thumba oil	Orifice plate	4.5:1	NaOH	1	30	45–55	80	Pal et al. (2010)
Used frying oil	Orifice plate	—	KOH	—	10	60	95	Ghayal et al. (2013)
Waste cooking oil (palm olein)	Orifice plate	6:1	KOH	1	15	60	98.1	Chuah et al. (2015)
Treated rubber seed oil	Orifice plate	6:1	KOH	1	18	55	96.5	Bokhari et al. (2016)
Frying oil	Orifice plate	4.5:1	KOH	0.55	20	45	93.86	Kolhe et al. (2017)
Waste cooking oil	High speed homogenizer	12:1	KOH	3	120	50	97	Mohod et al. (2017)
Waste frying oil	Venturi	6:1	KOH	1.1	8	63	95.6	Chitsaz et al. (2018)
Castor oil	Nozzle	6:1	KOH	1	100	30	80.4	Mistry et al. (2019)
Cannabis sativa oil	Orifice plate	6:1	KOH	1	20	60	97.5	Khan et al. (2020)
Xanthium spinosum Oil	Orifice plate	6:1	KOH	1	25	60	98.8	Asif et al. (2021a)
Pistacia khinjuk oil	Orifice plate	17:1	KOH	1	20	55	98	Asif et al. (2021b)
Safflower oil	Rotor–stator	8.36:1	KOH	0.94	1.06	—	89.11	Samani et al. (2021)
Soybean oil	Orifice plate	6:1	NaOH	0.5	20	60	97.20	Vera-Rozo et al. (2022)
Castor oil	Rotor–stator	8.15:1	KOH	0.74	29.38	48.43	96	This Study

the decrease in viscosity, density, and TAN as indicated in Table 5, determines the optimization objectives. The process variables are adjusted appropriately to achieve a high level of attractiveness. Numerical and graphical optimization techniques determined the optimal conditions. The established optimum parameters of 8.15:1 M:O, 1499 rpm, 29.38 min, 48.43 °C, and catalyst concentration of 0.74 wt.% (Fig. 10) resulted in a predicted biodiesel production yield of 95.36% and a predicted decrease in viscosity, density, and TAN of 94.66%, 5.097%, and 89.49%, respectively. An extra batch has been performed under the predicted optimal conditions. That yielded approximately 96% biodiesel with a concomitant decrease of viscosity, density, and TAN of approximately 95%, 5.12%, and 90.02%, respectively. Thus,

Table 7 Physico-chemical characteristics of the produced biodiesel (B100)

Test	Analysis standard Method	B100	Biodiesel standard characteristics	
			ASTM-D6751	EN14214
Kinematic viscosity at 40 °C (cSt)	ASTM D-445	9.64	1.9–6.0	3.5–5.0
Density at 15 °C (g/cm^3)	ASTM D-4052	0.9103	—	0.86–0.9
TAN (mg KOH/g oil)	ASTM D-974	0.12	< 0.8	< 0.5
Flash point (°C)	ASTM D-93	178	> 130	> 101
Calorific value (MJ/kg)	ASTM D-5865	39.992	—	> 32.9
Sulfur content (wt.%)	ASTM D-4294	Nil	< 0.05	< 0.01

Table 8 Physico-chemical characteristics of the prepared bio-/ptero-diesel blends (B6-B20)

Test	Analysis standard Method	B0	B6	B10	B20	ASTM D7467	Egyptian Petro-diesel standards
Kinematic viscosity at 40 °C (cSt)	ASTM D-445	2.74	4.16	4.9	5.22	1.9–4.1	1.6–7
Density at 15 °C (g/cm^3)	ASTM D-4052	0.8503	0.8607	0.8701	0.8751	—	0.82–0.87
TAN (mg KOH/g oil)	ASTM D-974	0.017	0.051	0.068	0.081	< 0.3	Nil
Flash point (^{o}C)	ASTM D-93	103	110	119	129	> 52	> 55
Calorific value (MJ/kg)	ASTM D-5865	44.38	44.00	43.18	42.11	—	> 44.3
Sulfur content (wt.%)	ASTM D-4294	0.2	0.17	0.13	0.1	—	< 1

that would confirm the validity of the predicted quartic model Eqs. (10–14). Moreover, according to El-Gendy et al. (2014), the recoded decrease in viscosity, density, and TAN confirms the effectiveness of the transesterification process and biodiesel purity.

It is important to note that there was a roughly 5.11-fold reduction in reaction time relative to our previously reported castor oil transesterification using KOH and methanol via the conventional mixing reactor (Aboelazayem et al. 2018). That yielded 97.82% biodiesel at optimum operating conditions of 0.73% catalyst concentration, 150 min, 5.4:1 M:O molar ratio, 320 rpm, and 64 °C (Aboelazayem et al. 2018).

Moreover, Table 6 illustrates the biodiesel yields from different sustainable oil feedstock using various hydrodynamic reactors, relative to our performed study. That declares the feasibility of the applied rotor–stator reactor applied in this study. The obtained biodiesel yield was comparable to what was reported by Bokhari et al. (2016) using a hydrodynamic cavitation reactor with an orifice plate. It is worth mentioning that the biodiesel yield obtained in this study is higher than that reported by Samani et al. (2021) using a rotor–stator hydrodynamic cavitation reactor by approximately 7%. The physical effect of the hydrodynamic reactor (cavitation) is what causes the insoluble reactants (oil and alcohol) to emulsify better and more, with a consequent increment in the reactants' contact surface area through the micro-turbulence that is created during cavitation (Gholami et al. 2021). Thus, this in turn increases the reaction rate (Farvardin et al. 2022). A benefit of hydrodynamic cavitation is the reduced duration of the process for biodiesel synthesis. Because of the cavitation on the rotor and the rapid fluid circulation between the rotor and stator, hydrodynamic cavitation reactors create a shear force in the liquid in addition to microbubbles production, which grow, and collapse quickly (Gholami et al. 2021). High-speed fluid circulation in these reactors improves the amount of stirring and reaction rate advancement, which shortens production times and boosts efficiency (Chuah et al. 2015).

Reaction kinetics and thermodynamics

In a ground-breaking step this study examined the kinetic and thermodynamic data obtained from the transesterification process applying rotor–stator hydrodynamic cavitation reactor at the developed optimal conditions. The quartic models developed using Design Expert software and RSM have been utilized to predict the kinetic data required for determining the kinetic parameters. The necessary kinetic data was obtained by performing tests at temperatures ranging from 40 to 70 °C and reaction durations ranging from 2 to 60 min, while maintaining other variables at their predicted optimal levels without any changes. A graph has been created to examine the relationship between the experimental data and an initial hypothesis of a second-order response. An investigation was conducted to fit the experimental data by plotting $\left| 1/(1-X) \right|$ against (t) throughout a time range of 2 to 60 min. The plot analysis has indicated that the reaction's rate constant is 0.23 M^{-1} min^{-1} under the optimum reaction conditions.

In addition, the thermodynamic parameters have been calculated as part of this study. The reaction rate constants have been calculated within a temperature range of 40 °C to 70 °C while maintaining the other variables at their predicted ideal values. The calculated reaction rate constants were employed to plot the Arrhenius equation. The values of the activation energy (E_a) and Arrhenius constant (i.e., the frequency factor) are found to be 18.77 kJ/mol and 6.32 M^{-1} min^{-1}, respectively.

Physico-chemical characteristics of the produced biodiesel

Table 7 indicates the assessment of the generated biodiesel's fuel properties in comparison to an Egyptian petro-diesel sample and the global biodiesel standards. The generated biodiesel's qualities are all very acceptable and satisfy the majority of the requirements, except for the viscosity. It can

therefore be considered a practical fuel and a substitute for petro-diesel. The elevated viscosity of biodiesel produced from castor oil has been previously reported by Aboelazayem et al. (2018), who attributed that to the presence of the hydroxyl group in ricinoleic acid.

The biodiesel TAN was greater than that of the petro-diesel sample, recording 0.12 and 0.017 mg KOH/g oil, respectively. Nevertheless, it is within the international biodiesel requirements. This suggests that the produced biodiesel will not result in corrosion or pump plugging, which would cause operational issues (Candeia et al. 2009). The most important criterion is that it is free of sulfur, so upon combustion, it will not emit SOx and will not lead to acid rains. Moreover, engine parts will not corrode as a result of its use. It has a high flash point, recording 178 °C, so it can be safely handled, stored, and transported.

Although the recoded high viscosity of 9.64 cSt (Table 7) implies that the biodiesel produced would not work as well in injection or atomization, it would still provide lubrication and protection for an engine's moving parts. In fact, the trend towards ultra-low sulfur diesel fuel (ULSD) has been troublesome in this regard; therefore, the high lubricity is especially beneficial in this regard (Knothe 2005). When high-viscosity fuel is used in diesel engines, it leads to sedimentation in the injection, insufficient combustion, and inappropriate fuel atomization (Farvardin et al. 2022). That could be resolved by its dilution with proper solvents or a higher concentration of petro-diesel (Aboelazayem et al. 2018).

This result suggests creating various blends of the bio- and petro-diesel (B6-B20). Table 8 illustrates their physico-chemical properties, which meet all the Egyptian petro-diesel standards and the international standard of bio-/petro- diesel blends. The viscosity and density of perto-diesel increased with biodiesel concentration, suggesting better lubricity. Furthermore, the viscosity and density of the generated bio-/petro- diesel (Table 8) are comparable to the conventional Egyptian petro-diesel standards (1.6–7 cSt). Therefore, the current engine can handle the produced blends without the need for hardware adjustments. However, the TAN increased with biodiesel concentration, but it was within the international standard (Table 8). The S-content decreased with biodiesel concentration (Table 8). That is very beneficial to the environment and engine performance. The flash point increased, while the calorific value decreased with biodiesel concentration (Table 8). But the flash point is within the standard range and the calorific value is still considerable.

Conclusion

The enhancement of biodiesel synthesis from castor oil using a self-manufactured cylindrical rotor–stator hydrodynamic cavitation reactor is being studied for the first time in this work. The transesterification process was statistically optimised using RSM, and optimal operating parameters were found to be 8.15:1 M:O, 1499 rpm, 29.38 min, 48.43 °C, and 0.74 wt% KOH catalyst concentration. This resulted in a 96% biodiesel and a corresponding drop of roughly 95%, 5.12%, and 90.02% in viscosity, density, and TAN, respectively. Additionally, the process's kinetics and thermodynamics were investigated in a pioneering step. The reaction was found to be pseudo-second order, with the activation energy, frequency factor, and reaction rate constant being 0.23 M^{-1} min^{-1}, 18.77 kJ/mol, and 6.32 M^{-1} min^{-1}, respectively.

The final biodiesel properties meet the requirements of the international standards (ASTM-D6751 and EN14214), except for the viscosity. Yet, upon the preparation of different bio-/petro-diesel blends, all properties are comparable to the international standard ASTM D7467 and the Egyptian-marketed petro-diesel. That recommends the application of sustainable and non-edible castor oil for biodiesel production via the designed rotor–stator hydrodynamic reactor. However, more research is being done right now to make the designed rotor–stator hydrodynamic reactor more efficient and possible. This is to speed up the transesterification of oil feedstock and get a higher-quality biodiesel yield with low energy use and a high cavitation yield. Furthermore, conducting further research on the cracking of the biodiesel produced is recommended to enable the creation of other types of bio-refineries, such as biojet, and enhance product quality flexibility to meet market demands.

Author contributions Mohamed Khater: Performed the biodiesel production process and helped in the implementation of the reactor; Omar Aboelazayem: Performed the process modeling, optimization and kinetic analysis; Abdallah R. Ismail: Supervised the biodiesel production part and performed all the physicochemical evaluation of biodiesel and bio-/petro-diesel blends; Aya Soliman: Designed and implemented the reactor; Salem A. Abu: Performed the statistical analysis; Nour Sh. El-Gendy: The corresponding author, put forth the idea of scientific research, conceived and designed research, supervised experimental work, validated the results, interpreted and discussed the results, and wrote the manuscript; Abbas Anwar Ezzat: Supervised the design and implementation of reactor, put together with El-Gendy the idea of the scientific research, conceived and designed the research; All authors have read and agreed to the published version of the manuscript.

Funding Open access funding provided by The Science, Technology & Innovation Funding Authority (STDF) in cooperation with The Egyptian Knowledge Bank (EKB).

Declarations

Conflict of interest All authors declare thath they have no conflict of interest.

References

ASTM. (2010). Annual Book of ASTM Standards. Petroleum Products and Lubricants (I–III), 05.01–05.03. West Conshohocken, PA: American Society for Testing and Materials.

ASTM Standard D6751. (2008). Standard specification for bio-diesel fuel (B100) blend stock for distillate fuels. ASTM, West Conshohocken, PA.

ASTM Standard D7467–15ce1. (2013). Standard Specification for Diesel Fuel Oil, Biodiesel Blend (B6 to B20). West Conshohocken, PA: American Society for Testing and Materials.

Aboelazayem O, El-Gendy NSh, Abdel-Rehim AA, Ashour F, Sadek MA (2018) Biodiesel production from castor oil in Egypt: process optimisation, kinetic study, diesel engine performance and exhaust emissions analysis. Energy 157:843–852. https://doi.org/10.1016/j.energy.2018.05.202

Angassa K, Tesfay E, Weldmichael TG, Kebede S (2023) Response surface methodology process optimization of biodiesel production from castor seed oil. J Chem. https://doi.org/10.1155/2023/6657732

Asif S, Klemeš JJ, Bokhari A, Chofreh AG (2021a) Pilot scale intensification of *Pistacia khinjuk* oil via chemical interesterification using hydrodynamic cavitation technology. Chem Eng Trans 89:277–282. https://doi.org/10.3303/CET2189047

Asif S, Klemeš JJ, Mukhtar A, Saqib S, Chuahe LF, Bokhari A (2021b) Intensification of biodiesel synthesis in a cavitation system from *Xanthium spinosum* oil. Chem Eng Trans 86:152–156. https://doi.org/10.3303/CET2186026

Attia AMA, Nour M, Nada SA (2018) Study of Egyptian castor biodiesel-diesel fuel properties and diesel engine performance for a wide range of blending ratios and operating conditions for the sake of the optimal blending ratio. Energy Convers Manag 174:364–377. https://doi.org/10.1016/j.enconman.2018.08.016

Bauddh K, Singh RP (2012) Growth, tolerance efficiency and phytoremediation potential of *Ricinus communis* (L.) and *Brassica juncea* (L.) in salinity and drought affected cadmium contaminated soil. Ecotoxicol Environ Saf 85:13–22. https://doi.org/10.1016/j.ecoenv.2012.08.019

Bokhari A, Chuah LF, Yusup S, Klemeš JJ, Akbar MM, Kamil RNM (2016) Cleaner production of rubber seed oil methyl ester using a hydrodynamic cavitation: optimisation and parametric study. J Clean Prod 136:31–41. https://doi.org/10.1016/j.jclepro.2016.04.091

Candeia RA, Silva MCD, Carvalho Filho JR, Brasilino MGA, Bicudo TC, Santos IMG (2009) Influence of soybean bio-diesel content on basic properties of bio-diesel-diesel blends. Fuel 88:738–743. https://doi.org/10.1016/j.fuel.2008.10.015

Carrino L, Visconti D, Fiorentino N, Fagnano M (2020) Biofuel production with castor bean: a win–win strategy for marginal land. Agronomy 10:1690. https://doi.org/10.3390/agronomy10111690

Chitsaz H, Omidkhah M, Ghobadian B, Ardjmand M (2018) Optimization of hydrodynamic cavitation process of biodiesel production by response surface methodology. J Environ Chem Eng 6(2):2262–2268. https://doi.org/10.1016/j.jece.2018.02.047

Chuah LF, Yusup S, Aziz ARA, Bokhari A, Klemeš JJ, Abdullah MZ (2015) Intensification of biodiesel synthesis from waste cooking oil (palm olein) in a hydrodynamic cavitation reactor: effect of operating parameters on methyl ester conversion. Chem. Eng. Process: Process Intensif. 95:235–240. https://doi.org/10.1016/j.cep.2015.06.018

Crudo D, Bosco V, Cavaglià G, Grillo G, Mantegna S, Cravotto G (2016) Biodiesel production process intensification using a rotor-stator type generator of hydrodynamic cavitation. Ultrason Sonochem 33:220–225. https://doi.org/10.1016/j.ultsonch.2016.05.001

El-Gendy NSh, Deriase SF, Osman DI (2014) The optimization of biodiesel production from waste frying oil using response surface methodology and the investigation of correlations for changes in basic properties of bio-petro-diesel blends. Energ Sources a: Recovery Util Environ Eff 36(5):457–470. https://doi.org/10.1080/15567036.2013.764360

Farvardin M, Samani BH, Rostami S, Abbaszadeh-Mayvan A, Najafi G, Fayyazi E (2022) Enhancement of biodiesel production from waste cooking oil: ultrasonic-hydrodynamic combined cavitation system. Energ Sources a: Recovery Util Environ Eff 44(2):5065–5079. https://doi.org/10.1080/15567036.2019.1657524

Felizardo P, Correia JN, Raposo I, Mendes JF, Berkemier R, Bordado JM (2006) Production of biodiesel from waste frying oils. Waste Manage 26:489–494. https://doi.org/10.1016/j.wasman.2005.02.025

Ghayal D, Pandit AB, Rathod VK (2013) Optimization of biodiesel production in a hydrodynamic cavitation reactor using used frying oil. Ultrason Sonochem 20(1):322–328. https://doi.org/10.1016/j.ultsonch.2012.07.009

Gholami A, Pourfayaz F, Saifoddin A (2021) Techno-economic assessment and sensitivity analysis of biodiesel production intensified through hydrodynamic cavitation. Energy Sci Eng 9:1997–2018. https://doi.org/10.1002/ese3.941

Gole VL, Naveen KR, Gogate PR (2013) Hydrodynamic cavitation as an efficient approach for intensification of synthesis of methyl esters from sustainable feedstock. Chem Eng Process: Process Intensif 71:70–76. https://doi.org/10.1016/j.cep.2012.10.006

Hamidi R, Damizia M, de Filippis P, Patrizi D, Verdone N, Vilardi G, de Caprariis B (2023) Recent developments and future outlooks of hydrodynamic cavitation as an intensification technology for renewable biofuels production. J Environ Chem Eng 11:110819. https://doi.org/10.1016/j.jece.2023.110819

Hanif M, Bhatti IA, Zahid M, Shahid M (2022) Production of biodiesel from non-edible feedstocks using environment friendly nano-magnetic Fe/SnO catalyst. Sci Rep 12:16705. https://doi.org/10.1038/s41598-022-20856-7

Innocenzi V, Prisciandaro M (2021) Technical feasibility of biodiesel production from virgin oil and waste cooking oil: comparison between traditional and innovative process based on

hydrodynamic cavitation. Waste Manage 122:15–25. https://doi.org/10.1016/j.wasman.2020.12.034

Ismail AR, El-Henawy SB, Younis SA, Betiha MAA, Amr SA, El-Gendy NSh, Azab MS, Sedky NM (2017) Optimization of a batch CaO-catalyzed transesterification of used domestic waste oil with methanol and elucidation of a mathematical correlation between biodiesel yield and percent conversion. Energ Sources a: Recovery Util Environ Eff 39(10):1013–1028. https://doi.org/10.1080/15567036.2017.1284958

JUS EN 14214. 2004. In: Automotive Fuels: Fatty Acid Methyl Esters (FAME) for Diesel Engines—Requirements and Test Methods. Belgrade, Serbia: Standardization Institute.

Khan IA, Prasad N, Pal A, Yadav AK (2020) Efficient production of biodiesel from *Cannabis sativa* oil using intensified transesterification (hydrodynamic cavitation) method, Energ. Sources a: Recovery Util Environ Eff 42(20):2461–2470. https://doi.org/10.1080/15567036.2019.1607946

Khater EG, AbdAllah SA, Bahnasawy AH, Abu Hashish HM (2023) Enhancing bio-oil yield extracted from Egyptian castor seeds by using microwave and ultrasonic. Sci Rep 13:4606. https://doi.org/10.1038/s41598-023-31794-3

Knothe G (2005) Dependence of biodiesel fuel properties on the structure of fatty acid alkyl esters. Fuel Process Technol 86:1059–1070. https://doi.org/10.1016/j.fuproc.2004.11.002

Kolhe NS, Gupta AR, Rathod VK (2017) Production and purification of biodiesel produced from used frying oil using hydrodynamic cavitation. Resour-Effic Technol 3:198–203. https://doi.org/10.1016/j.reffit.2017.04.008

María Elena, T.-D.C., Jose Luis, B.-M., VIDAL-SANTOS, Adrián, V.-S., Esther Guadalupe, N.-M. (2022). State of the art in the optimization of physico-chemical operating parameters of hydrodynamic cavitation reactors for the production of FAME J Technol Dev https://doi.org/10.35429/JTD.2022.17.6.1.8

Mistry, U., Thakkar, K., Kodgire, P., Kachhwaha, S.S., 2019. Biodiesel production from castor seeds (*Ricinus communis*) oil using hydrodynamic cavitation. ICTEA:International Conference on Thermal Engineering 1–3.

Mohod AV, Gogate PR, Viel G, Firmino P, Giudic R (2017) Intensification of biodiesel production using hydrodynamic cavitation based on high speed homogenizer. Chem Eng J 316:751–757. https://doi.org/10.1016/j.cej.2017.02.011

Mubofu EB (2016) Castor oil as a potential renewable resource for the production of functional materials. Sustain Chem Process 4:11. https://doi.org/10.1186/s40508-016-0055-8

Naderloo L (2020) Energy ratio of produced biodiesel in hydrodynamic cavitation reactor equipped with LabVIEW controller and artificial intelligence. Energy Rep 6:1456–1467. https://doi.org/10.1016/j.egyr.2020.05.029

Nassar HN, Abd El Salam HM, Al-Sadek AF, Abu Amr SA, El-Gendy NSh (2024) *para*-Nitrophenol nano-biodegradation using *Turbinaria triquetra*-synthesized magnetic nanoparticles-coated novel bacteria: a sustainable approach for refinery wastewater treatment. Int J Environ Sci Technol. https://doi.org/10.1007/s13762-024-05650-4

Nassar HN, Ismail AR, El-Salamony RA, Aboelazayem O, Abu Amr SA, El-Gendy NSh (2021) Animal bone affluence in environmental reclamation: biodiesel production, petro-diesel biodesulfurization and wastewater photo-treatment. Biofuels Bioprod Bioref 15:770–792. https://doi.org/10.1002/bbb.2194

Ortega-Alegria DR, Floréz-Marulanda JF (2019) Design and manufacturing of an ultrasonic reactor for biodiesel obtaining by transesterification. DYNA 86(211):75–83. https://doi.org/10.15446/dyna.v86n211.78518

Pal A, Verma A, Kachhwaha SS, Maji S (2010) Biodiesel production through hydrodynamic cavitation and performance testing. Renew Energ 35:619–624. https://doi.org/10.1016/j.renene.2009.08.027

Reşitoğlu IS, Altinişik K, Keskin A (2015) The pollutant emissions from diesel-engine vehicles and exhaust after treatment systems. Clean Techn Environ Policy 17:15–27. https://doi.org/10.1007/s10098-014-0793-9

Samani BH, Behruzian M, Najafi G, Fayyazi E, Ghobadian B, Behruzian A, Mofijur M, Mazlan M, Yue J (2021) The rotor-stator type hydrodynamic cavitation reactor approach for enhanced biodiesel fuel production. Fuel 283:118821. https://doi.org/10.1016/j.fuel.2020.118821

Samuel OD, Okwu MO, Amosun ST, Verma TN, Afolalu SA (2019) Production of fatty acid ethyl esters from rubber seed oil in hydrodynamic cavitation reactor: study of reaction parameters and some fuel properties. Ind Crops Prod 41:111658. https://doi.org/10.1016/j.indcrop.2019.111658

Sheehan, J., Camobreco, V., Duffield, J., Graboski, M., Shapouri, H. (1998) An overview of biodiesel and petroleum diesel life cycles. National Renewable Energy Laboratory, NREL/TP-580–24772, Available electronically at http://www.doe.gov/bridge

Tamilvanan A, Balamurugan K, Ponappa K, Kumar BM (2016) Using response surface methodology in synthesis of ultrafine copper nanoparticles by electrolysis. Int J Nanoscience 15(1–2):1650001. https://doi.org/10.1142/S0219581X16500010

Tamilvanan A, Jeyalakshmi P, Mohanraj M, Deepanraj B (2022) Feasibility study on raw *Simarouba glauca* oil as an alternate fuel in a diesel engine and comparative assessment with its esterified oil. Fuel 327:125168. https://doi.org/10.1016/j.fuel.2022.125168

Vera-Rozo JR, Riesco-Ávila JM, Poveda-Pachon MY, Zaleta-Aguilar A (2022) Biodiesel production by hydrodynamic cavitation through an orifice plate. Chem Eng Trans 92:565–570. https://doi.org/10.3303/CET2292095

Wu Z, Tagliapietra S, Giraudo A, Martina K, Cravotto G (2019) Harnessing cavitational effects for green process intensification. Ultrason Sonochem 52:530–546. https://doi.org/10.1016/j.ultsonch.2018.12.032

Xu H, Ou L, Li Y, Hawkins TR, Wang M (2022) Life cycle greenhouse gas emissions of biodiesel and renewable diesel production in the United States. Environ Sci Technol 56:7512–7521. https://doi.org/10.1021/acs.est.2c00289

Yusup S, Bokhari A, Chuah LF, Ahamd J (2015) Pre-blended methyl esters production from crude palm and rubber seed oil via hydrodynamic cavitation reactor. Chem Eng Trans 43:517–522. https://doi.org/10.3303/CET1543087